IEEE TRANSACTIONS ON

GEOSCIENCE AND REMOTE SENSING

A PUBLICATION OF THE IEEE GEOSCIENCE AND REMOTE SENSING SOCIETY

JUNE 2008 VOLUME 46 NUMBER 6 IGRSD2 (ISSN 0196-2892)

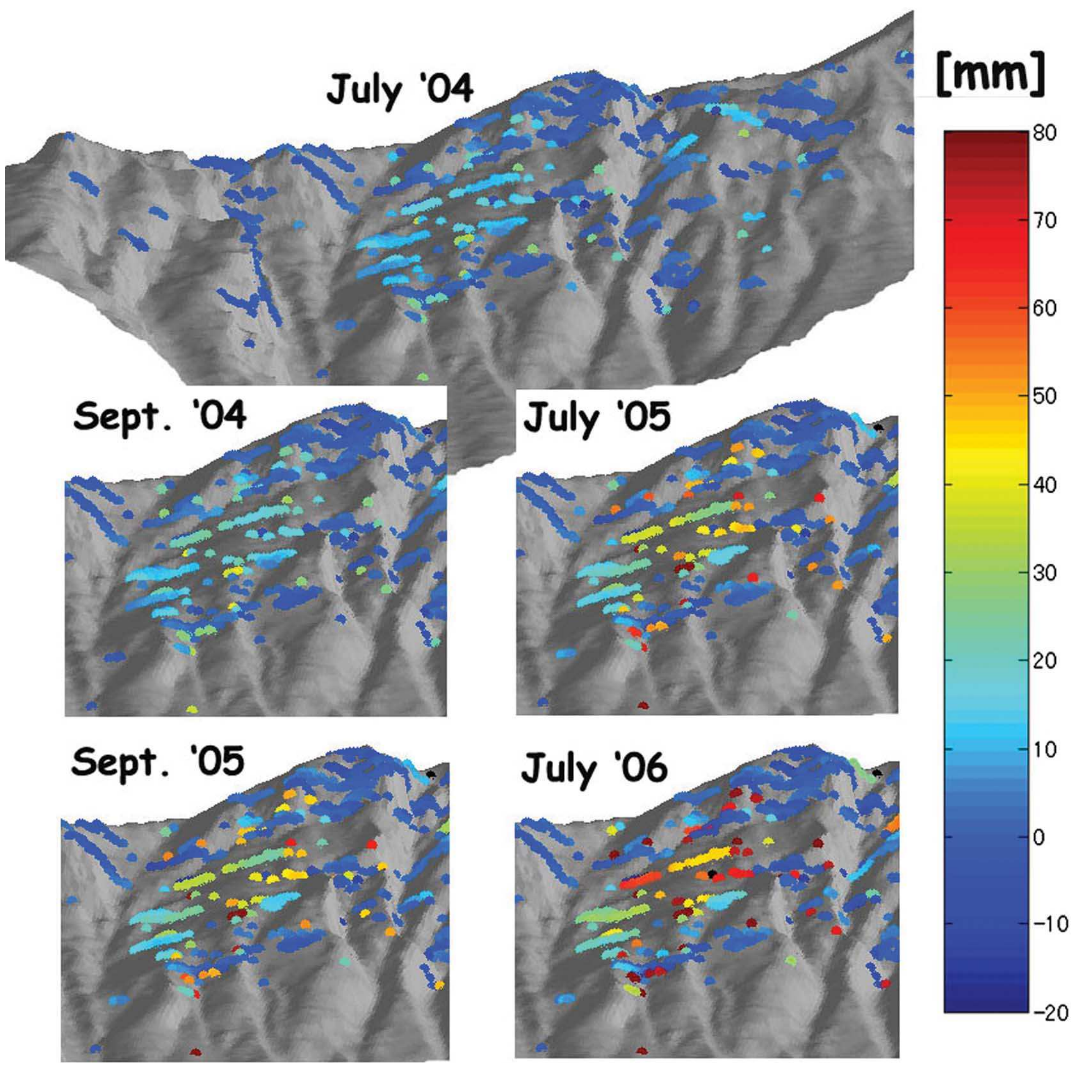

Six different ground-based SAR (GB-SAR) surveys were scheduled for monitoring an alpine landslide over a period of about three years. Here the maps represent the displacements along the line of sight detected at each survey with respect to the first survey in September 2003.

IEEE

IEEE TRANSACTIONS ON GEOSCIENCE AND REMOTE SENSING (ISSN 0196-2892) is published monthly by The Institute of Electrical and Electronics Engineers, Inc. Responsibility for the contents rests upon the authors and not upon the IEEE, the Society/Council, or its members. **IEEE Corporate Office:** 3 Park Avenue, 17th Floor, New York, NY 10016-5997. **IEEE Operations Center:** 445 Hoes Lane, Piscataway, NJ 08854-4141. **NJ Telephone:** +1 732 981 0060. **Price/Publication Information:** Individual copies: IEEE members $20.00 (first copy only), nonmembers $58.00 per copy. (Note: Postage and handling charge not included.) Member and nonmember subscription prices available on request. Available in microfiche and microfilm.

Periodicals Postage Paid at New York, NY, and at additional mailing offices. **Postmaster:** Send address changes to IEEE TRANSACTIONS ON GEOSCIENCE AND REMOTE SENSING, IEEE, 445 Hoes Lane, Piscataway, NJ 08854-4141. GST Registration No. 125634188. GST Registration No. 125634188. CPC Sales Agreement #40013087. Return undeliverable Canada addresses to: Pitney Bowes IMEX, P.O. Box 4332, Stanton Rd., Toronto, ON M5W 3J4, Canada. Printed in U.S.A.

Digital Object Identifier 10.1109/TGRS.2008.925328

IEEE TRANSACTIONS ON

GEOSCIENCE AND REMOTE SENSING

A PUBLICATION OF THE IEEE GEOSCIENCE AND REMOTE SENSING SOCIETY

JUNE 2008 VOLUME 46 NUMBER 6 IGRSD2 (ISSN 0196-2892)

PAPERS

Radar

Scattering

Electromagnetics

Radar Polarimetry

Rain, Clouds, and Aerosol

(Contents Continued on Page 1578)

(Contents Continued from Page 1577)

About the Cover: Ground-based SAR (GB-SAR) interferometry has been extensively used in monitoring applications in the last decade. It is based on the same principles as satellite SAR techniques. A GB-SAR sensor was used for monitoring a landslide moving only a few centimeters per year. The sensor was installed six times several months apart in time over the three-year observation period. Interferograms are formed by cross-combining images from different surveys, but reliable phase information can be obtained only on a limited ensemble of coherent pixels. The evolution of the landslide relatively to the selected pixels and across the surveys is retrieved in a least square sense without any assumptions on its regularity. Finally, the obtained maps represent the line-of-sight displacement detected at each survey with respect to the first survey in September 2003. For more information, please see "Analysis of Ground-Based SAR Data With Diverse Temporal Baselines," by Noferini *et al.*, which begins on page 1614.

Analysis of Ground-Based SAR Data With Diverse Temporal Baselines

Linhsia Noferini, Takuya Takayama, *Student Member, IEEE*, Massimiliano Pieraccini, Daniele Mecatti, Giovanni Macaluso, Guido Luzi, and Carlo Atzeni

***Abstract*—In this paper, the algorithms developed for satellite synthetic aperture radar (SAR) interferometry were adapted to the ground-based SAR (GB-SAR) configuration and used for detecting the displacements of an alpine landslide which have occurred over many years. Indeed GB-SAR interferometry is based on the same principles as satellite SAR techniques but benefits from the GB-SAR's versatility and capability of gathering many images per day. In monitoring applications of landslides moving only few centimeters per year, as the case here reported, the GB-SAR sensor is installed at repeated intervals several months apart over the observation period. Although the revisiting time is very similar to the satellite one, for each survey, lasting two or three days, more than ten images are available. They are analyzed separately and in combination with images from other surveys for coherent pixel selection. Interferograms are formed by cross-combining images from different surveys. Finally, the evolution of the deformation across the surveys is retrieved in a least square sense without any assumptions on its regularity. The used GB-SAR technique is described in detail in this paper, and the results obtained with regard to a landslide in the Italian Alps that has been monitored over a period of about three years are discussed.**

***Index Terms*—Atmospheric phase, ground-based synthetic aperture radar (GB-SAR) interferometry, landslide monitoring, persistent scatterers, 2-D phase unwrapping.**

I. Introduction

IN THE last decade, radar interferometric techniques have been successfully extended from space- to ground-based observations for monitoring mass terrain movements on a smaller scale and with improved spatial resolution [1]–[3]. Generally, a ground-based synthetic aperture radar (GB-SAR) is used for monitoring fast-moving landslides moving a few millimeters per day, as it can operate at a very high rate (even one image every 10 min). The sensors were kept working almost continuously from the same position, providing up-to-date displacement maps without topographic errors.

Slow-moving landslides (few centimeters per years) require a different approach that is more similar to the classic multipass interferometry. For these cases, GB-SAR surveys are planned several months apart (depending on the rate of deformation expected), and the instrumentation has to be installed and then dismounted each time. This leads to severe temporal decorrelation and, eventually, to geometric baseline errors as well [4]. Nevertheless, it is possible to overcome these difficulties as already reported in [5]. With respect to this previous work, where only data from subsequent surveys were compared for displacement mapping, here, the full temporal data set consisting of six different surveys was exploited at the same time similarly to the technique presented in [6] for the satellite case. Images gathered at different surveys were cross-combined in order to provide a larger time sampling of the deformation. The final displacement at each survey was determined in a least square sense according to this data set. The used model for the GB-SAR interferometric phase includes the phase due to displacement along the line of sight (LOS) and the propagation through the atmosphere [7], [8] being the zero-baseline configuration achieved, owing to the special instrumentation support designed by the authors [5]. Deviations from the estimated phase model were discussed regarding the problem of unwrapping [9] a sparse set of data with long temporal separation.

The analysis was carried out to a limited extent of pixels as it is the case with the permanent scatterers' technique [10], but in order to enlarge the pixel density, the GB-SAR's capability of gathering many images per day was exploited. Initially, the pixels were picked up if their amplitude dispersion indices [10] calculated through images within the same survey separately were all above the threshold. Then, they were tested at the end of the process and, eventually, removed by taking advantage of data redundancy in time.

The GB-SAR data processed here regard an alpine landslide located near Citrin (Aosta) in northern Italy. Data gathering took place from September 2003 until June 2006.

II. GB-SAR Surveys

Citrin Valley, located in the Gran Bernardo Mountains in the Alps of Valle d'Aosta, Italy, has been subject to slow landslide movement since a large precipitation event in October 2000. After a major collapse in that year, the landslide has been proceeding at a rate of few centimeters per year, downward to the Citrin torrent flowing at the bottom of the valley.

In order to monitor the slow terrain movements, six GB-SAR surveys were carried out over 36 months, more specifically in September 2003, July and September 2004, July and September 2005, and then September 2006. The surveys were all planned in the summer time because the area affected by the landslide remains snow covered through most part of the year.

Manuscript received November 16, 2007.

L. Noferini, M. Pieraccini, D. Mecatti, G. Macaluso, G. Luzi, and C. Atzeni are with the Department of Electronics and Telecommunications, University of Florence, 50139 Florence, Italy.

T. Takayama is with the Graduate School of Environmental Studies, Tohoku University, Sendai 980-8576, Japan.

Color versions of one or more of the figures in this paper are available online at http://ieeexplore.ieee.org.

Digital Object Identifier 10.1109/TGRS.2008.916216

TABLE I
MEASUREMENT PARAMETERS

Sep 2003	Jul 2004	Sep 2004	Jul 2005	Sep 2005	Sep 2006
29	19	21	32	33	10

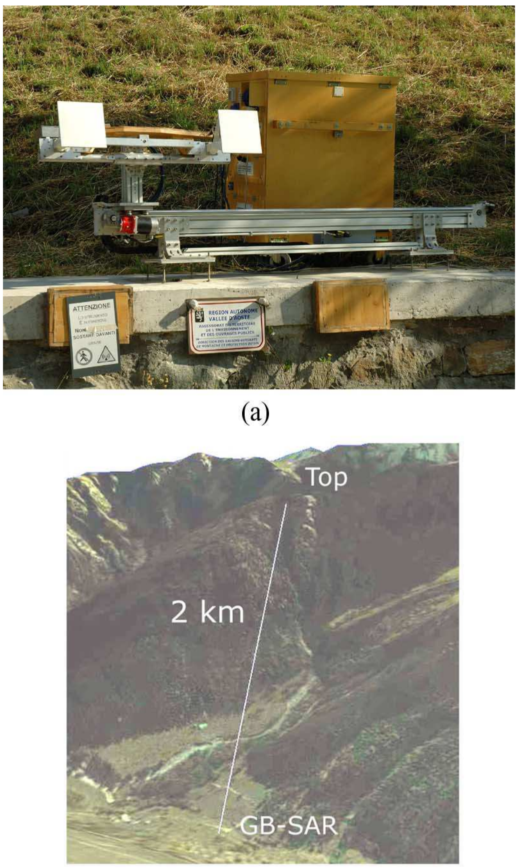

(a)

(b)

Fig. 1. (a) GB-SAR instrumentation. (b) Illumination geometry with a line connecting the radar location to the top of the monitored slope.

During the surveys, which lasted about two days each, dozens of images were collected (see Table I). Because no motion is expected within a survey, these images reflect temporal properties of the observed scene related to vegetation, daily changes of terrain wetness affecting the backscattered signal, and atmospheric variability.

The radar system mainly consists of a continuous-wave step-frequency transceiver working at C-band and of a couple of antennas (transmitting and receiving) mounted on a slide, which move along a rail, in order to synthesize the antenna aperture [5]. Fig. 1(a) shows the GB-SAR installed over a purposely built concrete basement in the chosen radar location. This was used to house a special support for exact repositioning of the instrumentation. One of the advantages of GB-SAR interferometry in comparison to satellite is that the radar sensor can easily be dismounted and reinstalled (with some precautions) on the same rail, thus achieving the zero-baseline configuration.

The radar location was chosen such as to ensure good coverage of the area to be monitored. The radar location with respect

TABLE II
NUMBER OF IMAGES ACQUIRED PER SURVEY

Polarization	VV
Target distance	1000 – 2000 m
Frequency bandwidth	30 MHz
Central frequency	5.85 GHz
Linear scanning length	1.8 m

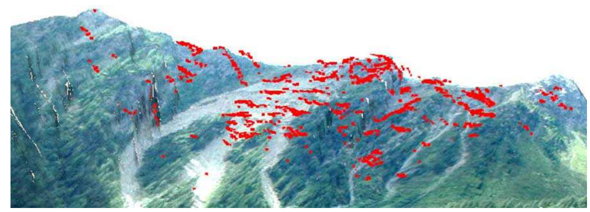

Fig. 2. Coherent pixels plotted on an optical picture. Coherent pixels distributed on rocks and vegetated areas are excluded almost completely.

to the slope to be monitored is shown in Fig. 1(b). It was about 2 km far from the top of the slope. From this location, the illuminated area on the slope is about 180 000 m^2, and across this area, the incidence angle varies from 50° up to 85°.

The same measurement parameters summarized in Table II were used for all of the surveys.

III. Pixel Selection

It is well known that, for applications involving long observation times (several years), most pixels in a SAR image suffer from time decorrelation and/or noise and, therefore, cannot be interferometrically processed. The identification of pixels that are coherent for a long time is a critical step in all the latest interferometric techniques [6], [10]–[12]. The amplitude dispersion index [10] or the coherence analysis [6] of sequences of images has been found to work successfully in identifying coherent pixels in satellite SAR interferometry. The same analysis can be applied to GB-SAR data collected at different surveys months apart, but the GB-SAR data set also consists of images taken within the same survey and, at a very fast rate, more than one per hour. This provides unusual additional information.

In this paper, in order to keep as much reliable pixels as possible, the procedure for selecting the coherent pixels is based on the analysis of images taken within the same survey without considering the effect of a longer temporal separation, which, instead, will be used later for refining the selection. The dispersion index [10] was calculated for the images within each survey separately, and pixels that showed the amplitude deviations smaller than a given threshold (0.3 in the current analysis) in all the surveys were picked up. By examining each survey separately, most of the vegetated areas can be identified and excluded from further analysis, but other sources of decorrelation with time, such as relative movement of the scatterers among different surveys, have no influence on the selection.

In Fig. 2, the pixels selected at this step are plotted on a 3-D model of the monitored slope with an optical picture overlapping it in order to determine where the selected pixels are distributed with respect to vegetated areas. It is evident that they are almost all on rocky areas that are lacking vegetation. They are about 10% of the number of available pixels in the image.

At this time, temporal properties among different surveys have not yet been exploited. Sections IV and V describe how the data behavior over a long period of time was used for refining the initial pixel selection.

IV. Phase Unwrapping

The images within each survey were combined, as described in the Appendix, in order to form phase maps representing the scene at the time of the surveys. Interferograms among the surveys were then generated by taking the differences among these phase maps. The unwrapping of the interferograms was carried out in two steps in order to reduce the occurrence of lost phase cycles. Generally, unwrapping techniques assume that absolute phase gradients among neighboring pixels fall within the interval $[-\pi, \pi)$. This limits the relative detectable movements and introduces errors that propagate over many pixels because of the unwrapping procedure. In order to set the intervals for the unknown phase gradients more properly, before applying the unwrapping procedure, a rough estimate of the pixel velocity was obtained by exploiting the wrapped data temporal properties.

A. Rough Estimation of Pixel Velocities

Generally, a differential interferometric phase model for satellite applications comprises the LOS motion, the elevation error compared to the used digital elevation model (DEM), and the atmospheric phase screen [10]. Those terms are estimated by exploiting data temporal properties, dependence on the normal baseline, and spatial properties, respectively. Because the GB-SAR sensor worked in the zero-baseline configuration, the term related to eventual DEM errors was erased from the used phase model. Indicating with $\varphi_k(x, r)$ the unwrapped phase of the pixel with range r and azimuth x, in the kth interferogram, the phase model for velocity estimation is

$$\varphi_k(x, r) = -\frac{4\pi}{\lambda} v(x, r)\Delta t_k + A_k x + B_k r + C_k + n_k(x, r) \tag{1}$$

where λ is the central transmitted wavelength, v is the LOS velocity, Δt_k is the lapse of time between the surveys combined to form the kth interferogram, A_k, B_k, and C_k determine the ramp approximating the atmospheric effect [8], [10] over the kth interferogram, and $n_k(r, x)$ is a noise component due to system noise or residual deviations from the model.

Because at this step, the interferograms were not yet unwrapped, the unknown quantities in (1) were estimated by means of periodogram functions for spectral analysis (see [13]). First, the coefficients describing the atmospheric effect were estimated over each interferogram looking for the frequencies of the periodogram associated to the variables x and r. Then, the estimated atmospheric effects were removed from the corresponding interferograms, and velocities were estimated by maximizing the following functional:

$$F(v) = \text{real}\left[\sum_{k=1}^{K} \exp(j\varphi_k) \exp\left(j\frac{4\pi}{\lambda} v\Delta t_k\right)\right] \tag{2}$$

where K is the total number of interferograms. Finding the maximum of the real part instead of the absolute value in (2) allows the reduction of the effect of the spurious peaks caused by a not regular and sufficiently dense time sampling. The velocities were obtained by limiting the velocity range from -1 to 4 cm/year, derived from the prior knowledge that the targets mainly move toward the radar with velocities of a few centimeters per year as a maximum. Positive velocities approach the radar. Fig. 3 shows the obtained LOS velocities of the selected pixels plotted on an available DEM.

In order to quantify how well the estimated phase model fitted with the measured phases, the coherence calculated according to (3) shown at the bottom of the next page was used.

Once more, the real part was used because it is more sensible to the exponents in (3). The coherence index (3) approaches 1 if a pixel is well represented by the estimated linear phase model (1). Fig. 4 shows the obtained coherence indices plotted on a DEM. High coherence index values are observed particularly at large rock faces, whereas small indices are observed particularly in the area labeled A in the figure, which is covered with relatively small rocks whose scattering characteristics are more sensitive to seasonal variations.

This index will be used in Section VI for the atmospheric phase effect compensation.

B. Phase Unwrapping Using the Velocities

The estimated velocities were used as input to the final unwrapping procedure. They provide additional information for solving the phase ambiguity more precisely.

The used phase unwrapping method is based on network flow programming for unwrapping sparse data [14]. First, neighboring pixels are defined according to their relative geometry, and then, the phase gradients among them are analyzed and, eventually, corrected before integrating them for the computation of an unambiguous solution.

Considering two neighboring pixels, the basic assumption used in this paper is that their phase gradient satisfies the following condition:

$$\left|\Delta\varphi_k + 2n\pi + \frac{4\pi}{\lambda}\Delta v\Delta t_k\right| < \pi \tag{4}$$

where $\Delta\phi_k$ is the wrapped phase gradient between the two pixels, directly derived from the kth interferogram, Δv is the velocity gradient obtained from the previous section, Δt_k is the lapse of time between the surveys compared in the kth interferogram, and $2n\pi$ are the unknown phase cycles to be added in order to satisfy (4).

This condition is highly recommended, in comparison to the standard one, which is (4) with $\Delta v = 0$, particularly when considering a large lapse of time and fast-moving pixels. For

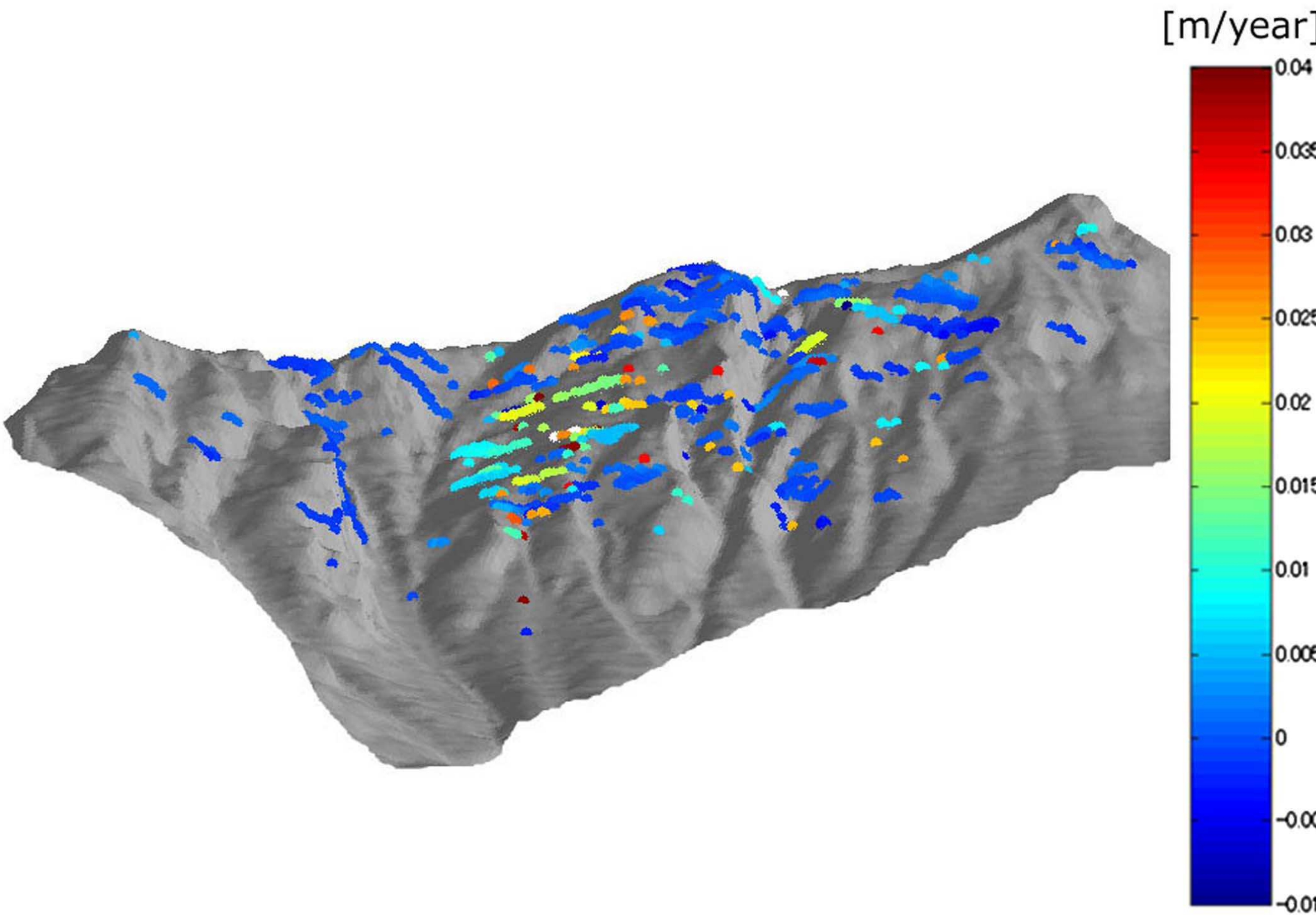

Fig. 3. LOS velocities estimated from the linear phase model are plotted on DEM.

instance, referring to the interferogram between the first and second surveys (ten months apart), the results of the unwrapping procedure satisfying condition (4) with $\Delta v \neq 0$ and $\Delta v = 0$ are shown in Fig. 5(a) and (b), respectively. In Fig. 5(b), the phase cycle losses are suspected between the sliding area A and the pixels above the white line drawn on the figure, which are stable rock faces. Indeed, because area A is supposed to move toward the radar and, therefore, corresponding to negative phases, the pixels on it should show smaller phases compared to the upper pixels. That the phase cycle losses cause a constant 2π phase offset error over all the pixels below the white line is evident.

V. Refinement of Pixel Selection

The 2-D phase unwrapping problem is solved so that the unwrapped spatial phase gradient will be an irrotational vector field. In order to assess the reliability of the final unwrapped interferograms, the irrotational property can also be required for the temporal dimension that was fully exploited in many techniques similar to those in [15]. For example, if ϕ_{ij} is the unwrapped interferogram between the ith and jth surveys, the irrotational property along with time among the first three surveys is

$$\phi_{12} + \phi_{23} + \phi_{31} = 0. \tag{5}$$

The integration of the obtained unwrapped phases along a temporal cycle path is zero if there are no unwrapping errors; otherwise, it yields into integral multiples of 2π.

In order to refine the initial pixel selection according to the unwrapping detected failures, pixels that did not satisfy the irrotational property along any temporal cycle path among those that can be built from the six available surveys were excluded.

$$\gamma = \mathrm{real}\left[\frac{\sum_{k=1}^{K} \exp(j\phi_k)\exp\left\{-j\left(-\frac{4\pi}{\lambda}v\Delta t_k + A_k x + B_k r + C_k\right)\right\}}{K}\right] \tag{3}$$

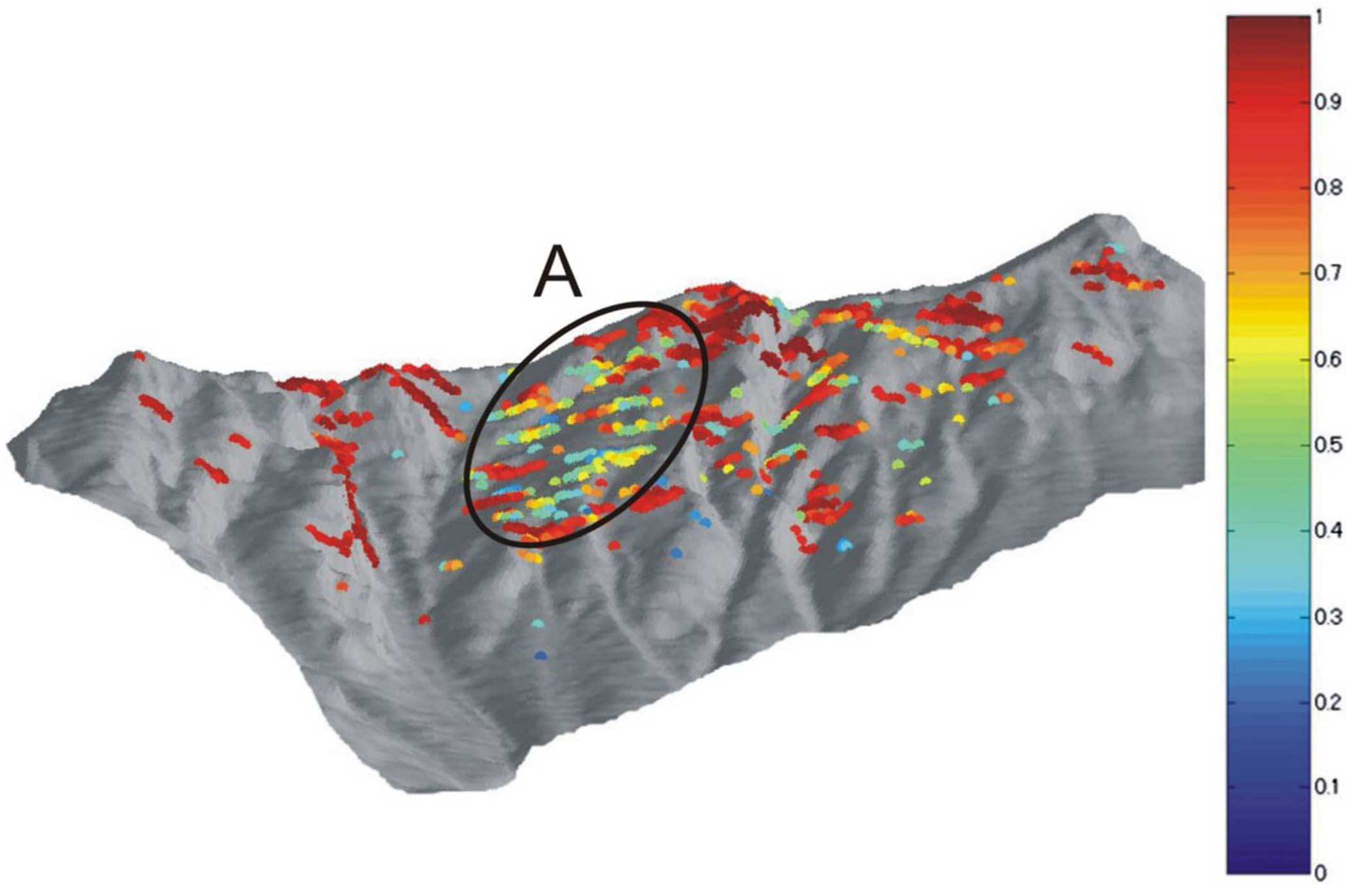

Fig. 4. Coherence index plotted on DEM. Pixels exhibit high dispersion index if the linear phase model (1) fits the interferometric phase well.

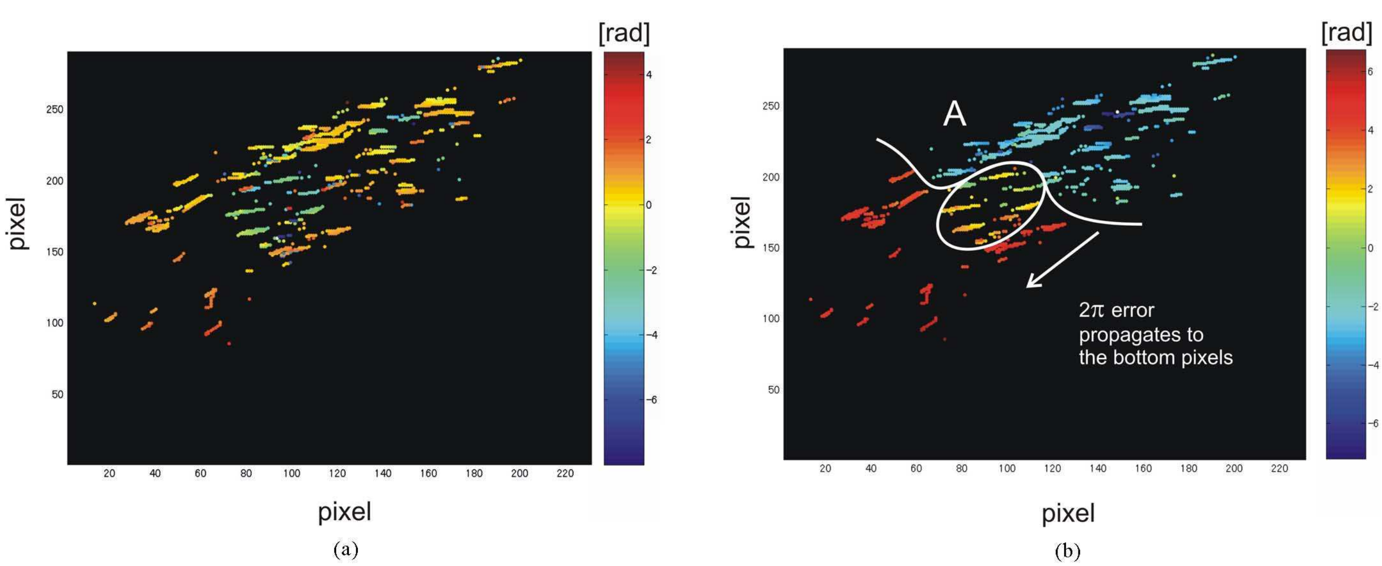

Fig. 5. Matrix of the interferometric phase between the first and second surveys (ten months apart) after 2-D unwrapping. For the initial estimate of phase gradients, (4) with $\Delta v \neq 0$ is imposed in (a), and (4) with and $\Delta v = 0$ is imposed in (b). Phase cycle losses between the highlighted area A and the pixels above the white line introduce phase error of 2π over all the pixels below the line.

Table III lists the ten independent integration cycle paths that can be built and the indices of the surveys included in the cycle. In Fig. 6, the pixels that did not satisfy the temporal irrotational property in at least one of the independent cycle paths are marked in red. Although the unwrapped interferometric phases of most of the selected pixels show temporal irrotational property, time inconsistency was detected in less than 4% of the pixels.

TABLE III
LIST OF ALL THE INDEPENDENT INTEGRATION CYCLE PATHS AND INDICES OF THE SURVEYS INCLUDED IN THE CYCLE

Cycle path index	Indexes of surveys in the cycle
1	1, 2, 3
2	1, 3, 4
3	2, 3, 4
4	2, 3, 5
5	3, 5, 6
6	3, 4, 6
7	2, 5, 6
8	4, 5, 6
9	1, 2, 5
10	1, 4, 6

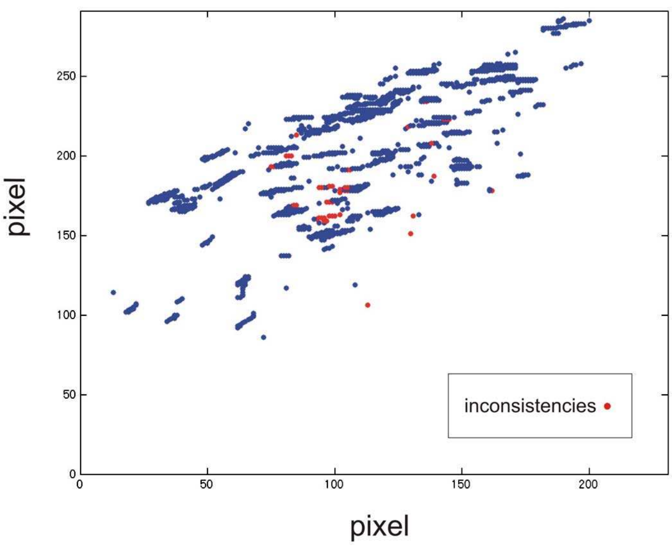

Fig. 6. Matrix showing time inconsistency after 2-D phase unwrapping.

Time inconsistencies, reflecting unwrapping errors, arise when phase gradients were estimated erroneously in at least one interferogram. The unwrapping procedure checks solutions depending on the rough velocity estimation discussed in Section IV-A. Errors on the estimated velocities are due to the fact that the observed motion largely differs from a linear motion or that, within that pixel, there are many distributed scatterers strongly decorrelating with time. In the latter case, the pixel cannot be interferometrically processed. Deviations from a linear motion more seriously affect the phase gradient estimation with the longer lapse of time Δt_k. Limiting the time lapse between surveys might reduce the number of pixels showing temporal inconsistency, but it also reduces the number of independent cycle paths for checking inconsistencies.

VI. NONLINEAR MOTION DETECTION

A. Estimation of the Parameters in the Model

In order to trace a nonlinear motion, interferograms must be processed without assumptions on its regularity. In comparison to phase model (1), in the phase model used at this step, the term containing the velocity is replaced by the observed

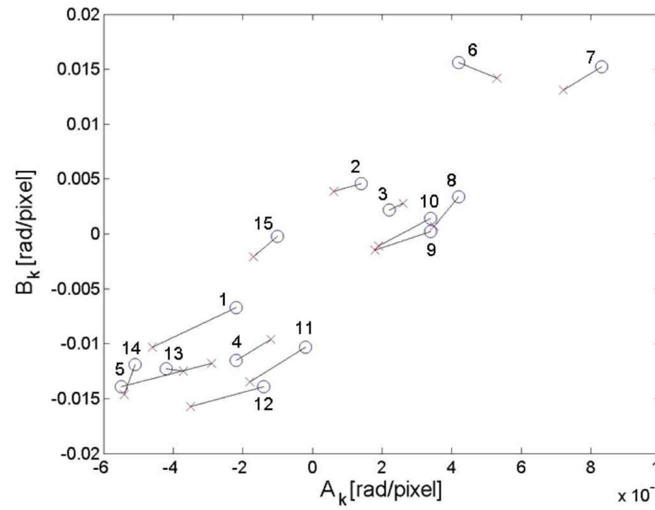

Fig. 7. Atmospheric coefficients estimated in Section IV-A (circle) and those finally estimated in Section VI-A (cross) for each interferogram. The number written above is the number of the corresponding interferogram.

LOS displacement Δd between the surveys combined in the unwrapped kth interferogram

$$\varphi_k(x, r) = -\frac{4\pi}{\lambda}\Delta d + A_k x + B_k r + C_k + n_k(x, r). \quad (6)$$

With the $M = 6$ surveys, a number $K = M(M-1)/2$ of different interferograms can be formed. If the number of pixels finally selected is N, all the K interferometric phases available for these pixels can be included in an $N \times K$ matrix $\mathbf{\Phi}$, and (6) can be rewritten in a matrix formulation as

$$\mathbf{\Phi} = -\frac{4\pi}{\lambda}(\mathbf{BD})^{\mathrm{T}} + \mathbf{AC} \quad (7)$$

where $\mathbf{D}$ is an $(M-1) \times N$ matrix, $M = 6$ is the number of surveys, with $\mathbf{D}_{i,j}$ representing the LOS displacement of the jth pixel at the time of the $(i+1)$th survey with respect to the first survey; $\mathbf{A}$ is an $N \times 3$ matrix which is composed of N rows, each containing the coordinates of a pixel and a constant value equals to 1 ($[x, r, 1]$); and finally, $\mathbf{C}$ is a $3 \times K$ matrix whose columns, $[A_k \;\; B_k \;\; C_k]^{\mathrm{T}}$, contain the coefficients describing the atmospheric phase ramp on the kth interferogram. The matrix $\mathbf{B}$ is a $K \times (M-1)$ matrix whose rows record the indices of the surveys used to generate each interferogram. It has $M-1$ columns only because the first survey was not included being the master. In this paper, $\mathbf{B}$ has the following form:

$$\mathbf{B} = \begin{bmatrix} 1 & 0 & \cdots & \cdots & 0 \\ 0 & 1 & \cdots & \cdots & 0 \\ \vdots & \vdots & \vdots & \vdots & \vdots \\ -1 & 1 & 0 & \cdots & 0 \\ \vdots & \vdots & \vdots & \ddots & \vdots \end{bmatrix} \quad (8)$$

which means, for example, considering the third filled row (the Mth of the matrix), that in the corresponding interferogram, the second survey was subtracted from the third survey.

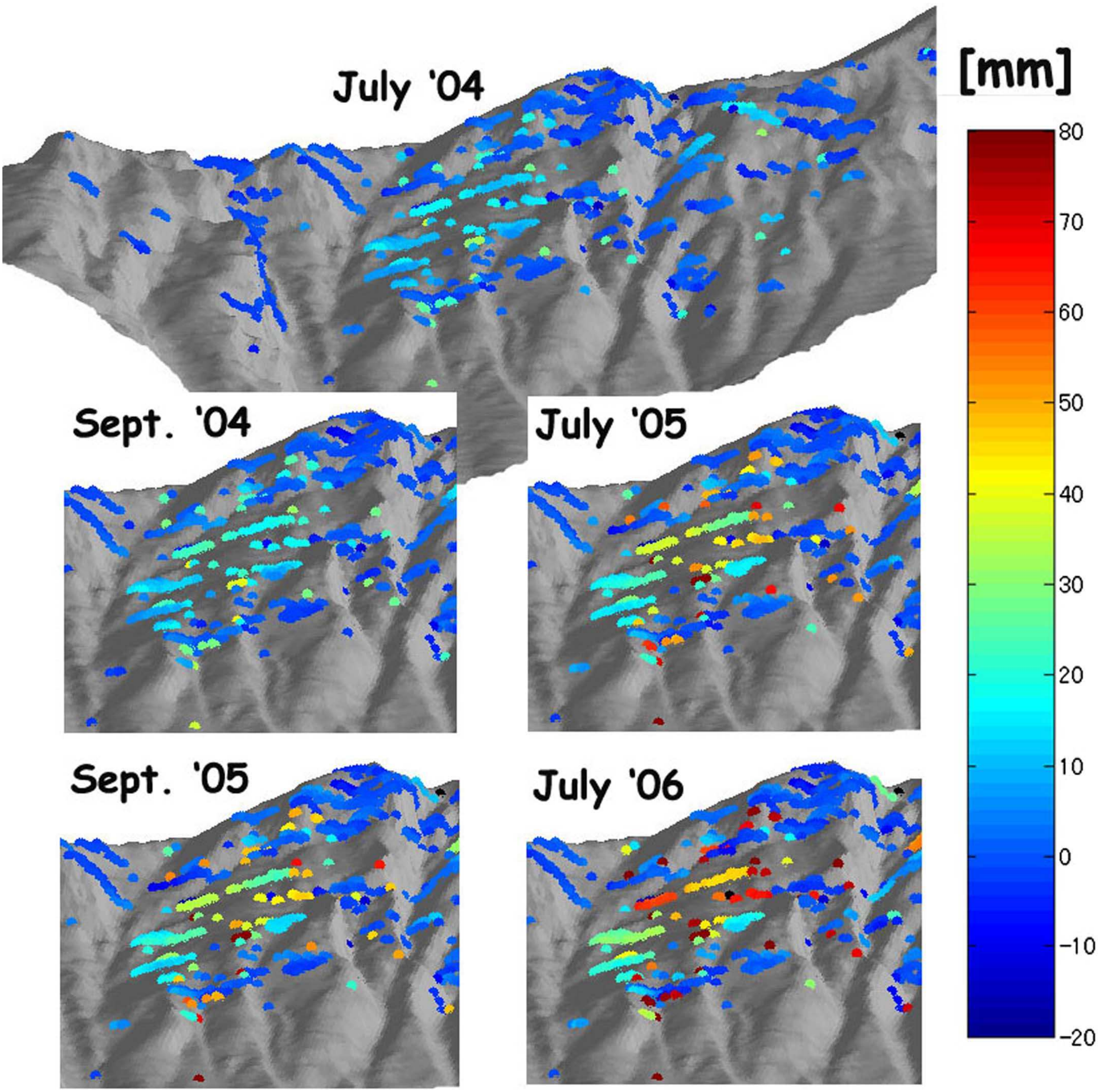

Fig. 8. Maps of the LOS displacements with respect to the first survey. Each map represents the displacements observed at the time of the survey.

Starting from (7), the atmospheric ramp coefficients and the displacement were estimated as follows.

1) Estimate the atmospheric phase coefficients on each interferogram. At this step, not all the pixels were considered, since the pixels whose interferometric phase contained a large motion component could cause a large atmospheric offset error. By using the rough estimation of the velocity previously discussed, those pixels which showed small velocity (see Fig. 3) and a large coherence index (see Fig. 4) were considered for the atmospheric estimation. The coefficients of the atmospheric ramp were estimated in a least square sense from (7) with all the displacement set to zero, as $\hat{\mathbf{C}} = (\mathbf{A}^{\mathbf{T}}\mathbf{A})^{-1}\mathbf{A}^{\mathbf{T}}\boldsymbol{\Phi}$.
2) The estimated atmospheric phase ramps were removed from the corresponding interferograms, and the displacement matrix $\mathbf{D}$ was estimated in a least square sense as

$$\mathbf{D} = \frac{\boldsymbol{\lambda}}{\mathbf{4}\boldsymbol{\pi}}(\mathbf{B}^{\mathbf{T}}\mathbf{B})^{-\mathbf{1}}\mathbf{B}^{\mathbf{T}}(\boldsymbol{\Phi} - \mathbf{A}\hat{\mathbf{C}})^{\mathrm{T}}.$$

The procedure can be iterated, but in this paper, it ran only one time because the results showed perfect matching to the phase model (6) without iteration if the atmospheric effect is precisely estimated, as explained in step 1, and the unwrapped phase satisfies the temporal irrotational property, as discussed in Section V.

B. Results

The results of the procedure presented in this paper were obtained by exploiting the 15 different interferograms formed by combining the six surveys. In order to estimate the atmospheric phase ramp, pixels exhibiting velocity slower than 2 mm/year and the phase dispersion index larger than 0.7 were considered. In Fig. 7, both the atmospheric coefficients estimated in Section IV-A from the wrapped interferograms considering all the early selected pixels and those estimated from the unwrapped interferograms considering only the pixels with low velocity and high degree of coherence are plotted for each interferogram. The coefficient unit is radians per pixel because the coordinates x and r are measured in pixels in the computations. The atmospheric effect above the monitored area is generally more than 1 rad.

The final maps of the observed LOS displacements are shown in Fig. 8. The area mostly affected by the landslide is very distinguishable from the rest of the pixels.

From the series of maps, the time behavior of each pixel can easily be analyzed by picking up the pixel and plotting its displacements. In Fig. 9, the LOS displacements with the time of the three pixels highlighted on the picture are plotted together. The pixels A and B are located where an active land movement is expected, whereas pixel C is on a stationary rock exposed on the top of the mountain.

In order to assess the reliability of the estimated displacements, the deviations of the phase model from the measured data were analyzed. The deviation of the ith pixel is given by

$$\sigma_i = \sqrt{\frac{\sum_{k=1}^{K} \left(\Phi_{ik} - \frac{4\pi}{\lambda} B_{kl} D_{li} - A_{ip} C_{pk}\right)^2}{K-1}}. \tag{9}$$

The result showed perfect matching, with the model being the deviation (9) less than 3×10^{-7} rad for all the pixels. If all the pixels were included for the atmospheric phase estimation, larger phase dispersion (from 0.01 to 0.08 rad) would be observed; moreover, the displacement of targets would be underestimated since part of the contribution to the phase due to velocity was misinterpreted as atmospheric component.

VII. CONCLUSION

In this paper, the results of landslide monitoring campaigns conducted over three years using a GB-SAR interferometer are reported. The radar system was mounted six times, several months apart, in order to survey the area affected by the landslide at very different times. Making use of the wide range of temporal baselines available within the collected data, from a few days to a few years, coherent pixel candidates were at first selected by exploiting the amplitude dispersion within each survey, and in the end, pixels were picked up by checking inconsistency with time.

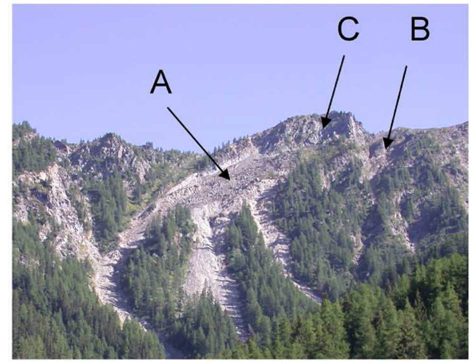

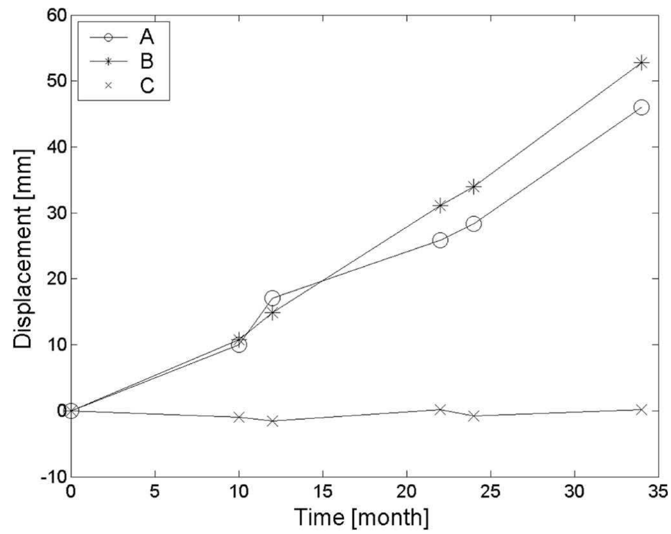

Fig. 9. LOS displacements with time observed at some representative points highlighted on the picture. A and B points are on areas where a fast movement is expected, and C is on a stable rock.

In order to prevent a phase cycle loss, the 2-D phase unwrapping was implemented by using an approximated prior knowledge of the pixel velocity. Finally, a phase model comprised of LOS displacements and atmospheric phase ramps was solved in minimum least square sense. The estimated phases well fit with the measured data.

APPENDIX
GENERATING THE INTERFEROGRAMS

Because many GB-SAR images are available for each survey, a large number of interferograms could be generated, but to have a single phase map for each survey is the most convenient solution in terms of calculation efficiency.

In order to enhance the signal-to-noise ratio of the maps representing the surveys, the maps must be formed by properly combining the images within the same survey.

The additive noise of a survey map could be reduced by taking the complex mean of the available images if atmospheric effects, which translate into random rotations, were negligible; otherwise, image phasors could even combine with opposite directions, deteriorating the signal-to-noise ratio. Because atmospheric effects do not influence the phase quality directly, instead of the complex images, their phases can be considered. Before using phases in the computations, they need to be unwrapped. In each survey, an image is taken as a master, and the phases of the other images are unwrapped with respect to the master. Indicating the nth and the master image of the mth survey with f_{mn} and f_{m1}, respectively, in this paper, the phase map representing this survey is obtained by

$$\phi_m = \frac{1}{N_m} \sum_{n=1}^{N_m} \left[\arg(f_{m1}) + \mathrm{PU}\left\{\arg\left((f_{mn} f_{m1}^*)\right)\right\}\right] \qquad (10)$$

where N_m is the total number of available images in mth survey and PU represents the 2-D phase unwrapping operator. Unwrapping was carried out over the selected pixels according to the techniques proposed in [14]. Images within the same survey generally show a high degree of coherence due to the short temporal baseline (less than a few days); therefore, the 2-D phase unwrapping can always be successfully carried out. Practically, (10) is the mean of the unwrapped phases with respect to the master of the images within the survey. It contains information about the target-sensor distance, noise, and a kind of average atmospheric effect over the survey period.

Final interferograms were then generated by taking the difference between two phase maps. A number of $K = 15$ different interferograms were formed by combining the six phase maps available.

ACKNOWLEDGMENT

The equipment used in this paper has been designed and constructed with the support of IDS-Ingegneria dei Sistemi SpA, Pisa (Italy), and it remains the property of this company.

REFERENCES

[1] M. Pieraccini, N. Casagli, G. Luzi, D. Tarchi, D. Mecatti, L. Noferini, and C. Atzeni, “Landslide monitoring by ground-based radar interferometry: A field test in Valdarno (Italy),” *Int. J. Remote Sens.*, vol. 24, no. 6, pp. 1385–1391, Sep. 2002.

[2] D. Leva, G. Nico, D. Tarchi, J. Fortuny, and A. J. Sieber, “Temporal analysis of a landslide by means of a ground-based SAR interferometer,” *IEEE Trans. Geosci. Remote Sens.*, vol. 41, no. 4, pp. 745–752, Apr. 2003.

[3] G. Antonello, N. Casagli, P. Farina, D. Leva, G. Nico, A. J. Sieber, and D. Tarchi, “Ground-based SAR interferometry for monitoring mass movements,” *Landslides*, vol. 1, no. 1, pp. 21–28, Mar. 2004.

[4] H. A. Zebker, J. Villasenor, and S. Hensley, “Decorrelation in interferometric radar echoes,” *IEEE Trans. Geosci. Remote Sens.*, vol. 30, no. 5, pp. 950–959, Sep. 1992.

[5] L. Noferini *et al.*, “Permanent scatterers analysis for atmospheric correction in ground based SAR interferometry,” *IEEE Trans. Geosci. Remote Sens.*, vol. 43, no. 7, pp. 1459–1471, Jul. 2005.

[6] P. Berardino, G. Fornaro, R. Lanari, and E. Sansosti, “A new algorithm for surface deformation monitoring based on small baseline differential SAR interferograms,” *IEEE Trans. Geosci. Remote Sens.*, vol. 40, no. 11, pp. 2375–2383, Nov. 2002.

[7] H. A. Zebker, P. A. Rosen, and S. Hensley, “Atmospheric effects in interferometric synthetic aperture radar surface deformation and topographic maps,” *J. Geophys. Res.*, vol. 102, no. B4, pp. 7547–7563, Apr. 10, 1997.

[8] L. Pipia, X. Fabregas, A. Aguasca, and J. J. A. Mallorqui, “Comparison of different techniques for atmospheric artifact compensation in GB-SAR differential acquisitions,” in *Proc. IGARSS*, Denver, CO, Aug. 2006, pp. 3739–3742.

[9] D. C. Ghiglia and M. D. Pritt, *Two-Dimensional Phase Unwrapping. Theory, Algorithms and Software*. New York: Wiley, Apr. 1998.

[10] A. Ferretti, C. Prati, and F. Rocca, “Permanent scatterers in SAR interferometry,” *IEEE Trans. Geosci. Remote Sens.*, vol. 39, no. 1, pp. 8–20, Jan. 2001.

[11] A. Hooper, H. A. Zebker, P. Segall, and B. Kampes, “A new method for measuring deformation on volcanoes and other natural terrains using InSar persistent scatterers,” *Geophys. Res. Lett.*, vol. 31, no. 23, p. L23 611, 2004. DOI:10.1029/2004GL021737.

[12] C. Werner, U. Wegmuller, T. Strozzi, and A. Wiesmann, “Interferometric point target analysis for deformation mapping,” in *Proc. IGARSS*, Toulouse, France, Jul. 2003, pp. 4362–4364.

[13] A. Ferretti, C. Prati, and F. Rocca, “Non linear subsidence rate estimation using permanent scatterers in differential SAR interferometry,” *IEEE Trans. Geosci. Remote Sens.*, vol. 38, no. 5, pp. 2202–2211, Sep. 2000.

[14] M. Costantini and P. A. Rosen, “A generalized phase unwrapping approach for sparse data,” in *Proc. IGARSS*, Hamburg, Germany, Jun. 1999, pp. 267–269.

[15] M. Costantini, F. Malvarosa, F. Minati, L. Pietranera, and G. Milillo, “A three-dimensional phase unwrapping algorithm for processing of multitemporal SAR interferometric measurements,” in *Proc. IGARSS*, Toronto, ON, Canada, Jun. 2002, vol. 3, pp. 1741–1743.

Linhsia Noferini received the degree in physics and the Ph.D. degree in engineering of electronic systems from the University of Florence, Florence, Italy, in 1999 and 2005, respectively.

She is currently working in a postdoctoral position with the Laboratory of Technologies for Cultural Heritage (TchLab) of the Department of Electronics and Telecommunications, University of Florence. Her research activities have focused mainly on processing data gathered from different measurement systems based on the use of a continuous-wave step-frequency radar. These electronic systems have been developed at the TchLab specifically for different kinds of applications: the monitoring of landslides, the monitoring of dams, the construction of digital models of terrain, the monitoring of snow covers, the monitoring of movements of glaciers, and finally wall investigation. She studied and implemented various interferometric SAR techniques. Often, her work has focused on the adaptation of the techniques developed for the satellite SAR sensors for the radar configuration based on the ground (GB-SAR) actually used by the research team of which she is part.

Takuya Takayama (S’06) received the B.E. degree in mechanical engineering and the M.E. degree in geosciences engineering from Tohoku University, Sendai, Japan, in 2004 and 2006, respectively. He is currently working toward the Ph.D. degree in the Graduate School of Environmental Studies, Tohoku University, working on the development of a directional borehole radar system.

From November 2006 to June 2007, he was with the Laboratory of Technology for Cultural Heritage, Florence University, Florence, Italy, through the Italian Government scholarship, working on the processing of the interferometric ground-based SAR data for the terrain monitoring.

Massimiliano Pieraccini received the degree in physics and the Ph.D. degree in nondestructive testing from the University of Florence, Florence, Italy, in 1994 and 1998, respectively.

Since 1995, he has been with the Department of Electronics and Telecommunications, University of Florence, where he was a Researcher from 1997 to 2005 and has been an Associate Professor since 1997. He has taught “Basic Electronics” and “Electronics for Telecommunications” with the Engineering Faculty, University of Florence. He has been a Research Manager for a number of research projects in the field of radar applications founded by the Ministry of Research, the National Research Council, and the European Community. He has authored several papers published in international journals and is a holder of three patents. His research interests included optoelectronic sensors and ultrasound transducers. Currently, he is dealing with synthetic aperture radar and ground-penetrating radar.

Prof. Pieraccini was the recipient of the Nello Carrara Degree Prize.

Daniele Mecatti was born in Florence, Italy, in 1974. He received the degree in electronic engineering and the Ph.D. degree in electronic systems engineering from the University of Florence, Florence, Italy, in 2001 and 2006, respectively. He discussed a doctoral thesis entitled "Interferometric radar for ground-based monitoring of unstable slopes." From 2001 to 2003, he attended a course on "monitoring techniques of cultural heritage" in the framework of the PARNASO Project of the Italian Ministry of Research.

He has been a Researcher with the Department of Electronics and Telecommunications, University of Florence, since April 2007. He has authored several papers published in international journals. He is currently working on synthetic aperture radar, interferometric radar techniques, and ground-penetrating radar prototype development.

Giovanni Macaluso was born in Prato, Italy, in 1973. He received the degree in electronic engineering and the Ph.D. degree in electronics systems engineering from the University of Florence, Florence, Italy, in 2002 and 2007, respectively.

He is currently with the Department of Electronics and Telecommunications, University of Florence, working on the application of interferometric synthetic aperture radar and ground-penetrating radar, with emphasis on the processing of acquired data. During his Ph.D., he was also collaborating on the experimentation of ground-based synthetic aperture interferometric radar systems for monitoring of landslides, glaciers, and snow-covered slopes.

Guido Luzi received the Honors degree in applied physics and the Ph.D. degree in electronic systems engineering from the University of Florence, Florence, Italy, in 1986 and 2003, respectively.

Since 1987, he has been working in microwave remotes sensing, active and passive, both in industrial and research institutions. Since 2000, he has been with the Department of Electronics and Telecommunications, University of Florence, where he is involved in the design and experimentation of radar-based sensing techniques for cultural heritage and environmental monitoring with emphasis on GB-SAR interferometry. He has dedicated his research activity to the development and experimentation of microwave sensors, taking part in numerous international remote sensing campaigns (AGRISCATT, AGRISAR, MACEUROPE) and within European Programs (EPOCH, MEDALUS, ENVIRONMENT, GALAHAD). He has also investigated innovative applications, focusing his interest toward geophysical and civil applications. He has authored or coauthored several papers concerning the aforementioned topics.

Carlo Atzeni has been a Full Professor of microelectronics with the University of Florence, Florence, Italy, since 1980, after his 15-year activity with the Electromagnetic Research Institute of the Italian National Research Council. His previous scientific activity was mainly concerned with signal and image processing, with emphasis on the development of microwave radar systems and ultrasound imaging systems for medical diagnostics. More recently, he organized and directed research projects applying microwave and laser imaging technologies to cultural heritage conservation and survey of environment. He has established the Laboratory of Technology for Environmental and Cultural Heritage, where a number of advanced activities are currently developed, such as optical 3-D acquisition for high-quality digital modeling of heritage artworks, microwave interferometry for static and dynamic monitoring of architectural structures and landslide instabilities, and synthetic aperture radar for underground and intrawall inspection.